JASA ARTICLE

Effect of wavy trachea walls on the oscillation onset pressure of silicone vocal folds

Patrick Häsner,[1] Andreas Prescher,[2] and Peter Birkholz[1,a)]
[1]Insitute of Acoustics and Speech Communication, Technische Universität Dresden, Germany
[2]Institute of Molecular and Cellular Anatomy, Aachen University Hospital, Aachen, Germany

ABSTRACT:
The influence of non-smooth trachea walls on phonation onset and offset pressures and the fundamental frequency of oscillation were experimentally investigated for three different synthetic vocal fold models. Three models of the trachea were compared: a cylindrical tube (smooth walls) and wavy-walled tubes with ripple depths of 1 and 2 mm. Threshold pressures for the onset and offset of phonation were measured at the lower and upper ends of each trachea tube. All measurements were performed both with and without a supraglottal resonator. While the fundamental frequency was not affected by non-smooth trachea walls, the phonation onset and offset pressures measured right below the glottis decreased with an increasing ripple depth of the trachea walls (up to 20% for 2 mm ripples). This effect was independent from the type of glottis model and the presence of a supraglottal resonator. The pressures at the lower end of the trachea and the average volume velocities showed a tendency to decrease with an increasing ripple depth of the trachea walls but to a much smaller extent. These results indicate that the subglottal geometry and the flow conditions in the trachea can substantially affect the oscillation of synthetic vocal folds.
 https://doi.org/10.1121/10.0003362

(Received 29 September 2020; revised 16 December 2020; accepted 29 December 2020; published online 21 January 2021)
[Editor: Zhaoyan Zhang] Pages: 466–475

I. INTRODUCTION

Synthetic, self-oscillating vocal fold models have become a valuable tool in voice research. Because the properties of these models can be selectively varied, they allow one to study the effect of specific geometric or biomechanical variations of the vocal folds or the surrounding structures on the vibration patterns and the resulting voice. Various factors of influence have been considered in previous studies with synthetic vocal folds, e.g., the effects of nonlinear vs linear material properties (Shaw *et al.*, 2012; Xuan and Zhang, 2014), simplified vs more realistic model geometries (Migimatsu and Tokuda, 2019; Pickup and Thomson, 2010), multiple vocal fold layers with different material properties (McPhail *et al.*, 2019; Mendelsohn and Zhang, 2011; Murray and Thomson, 2012), asymmetries between the left and right vocal folds (Bouvet *et al.*, 2021; Migimatsu and Tokuda, 2019; Pickup and Thomson, 2009), and including the ventricular folds above the vocal folds (Kniesburges *et al.*, 2017). Beyond basic voice research like this, synthetic vocal folds can be used as the voice source for physical speaking machines or robots (Birkholz *et al.*, 2019b; Fukui *et al.*, 2012).

An important part of all experimental setups for synthetic vocal folds is the subglottal system. Zhang *et al.* (2006, 2009) showed that models of the subglottal system should be carefully designed and have acoustic properties similar to the human subglottal system for the experimental results to be relevant for human phonation. In consequence, the length of the tracheal tube should be in the range of the length of the human trachea (Migimatsu and Tokuda, 2019). If a much longer subglottal tube is used instead, this may cause unwanted acoustics–structure interactions like the entrainment of vocal fold vibration with one of the subglottal resonances (Birkholz *et al.*, 2019a; Zhang *et al.*, 2006).

Compared to the influence of the *acoustic* properties of the subglottal system on vocal fold vibrations, the influence of the subglottal *flow patterns* has not been studied yet. Previous studies with synthetic vocal folds typically used a straight tracheal tube with smooth walls and a circular (Burks *et al.*, 2020; Migimatsu and Tokuda, 2019) or rectangular (McPhail *et al.*, 2019; Thomson *et al.*, 2005) cross section. In these tubes, a more or less laminar flow is expected based on the Reynolds' number. However, the *human* trachea is a noncylindrical tube with very irregular walls (Dekker, 1961). For quasi-static conditions with a permanently open glottis (as for breathing), the influence of realistic subglottal geometries on the flow has been studied both experimentally (Dekker, 1961) and with computer simulations (Choi *et al.*, 2009; Nowak *et al.*, 2003). These studies indicate that the airflow in the trachea is mostly turbulent instead of laminar during the greater part of normal respiration. Dekker (1961) determined a critical expiratory airflow of 122 cm^3/s at which the tracheal airflow becomes turbulent. Given that the peak glottal flow during modal phonation of male speakers is about 400 cm^3/s (Stevens, 1998), it is highly probable that the tracheal airflow is also turbulent during phonation at least for a part of the glottal oscillation

a)Electronic mail: peter.birkholz@tu-dresden.de

https://doi.org/10.1121/10.0003362

cycles. These flow conditions may affect vocal fold oscillations in a way that has been previously neglected in experiments with synthetic vocal folds.

A non-laminar flow in the trachea can have different reasons, e.g., the mixture of the expiratory airflow from the left and right main bronchi or the non-smooth tube walls. In this study, we explored the effect of the trachea walls. The trachea is about 12 cm long and has 12–20 *C*-shaped cartilaginous rings anteriorly and laterally, which are connected with soft tissue. The posterior side is formed by a membranous wall containing the nonstriated trachealis muscle (Breatnach *et al.*, 1984; Premakumar *et al.*, 2018). Depending on the longitudinal stretching or compression of the trachea, the walls form a more or less wavy pattern in which the cartilage rings and the tissue in between form the maxima and minima of the waves (Fischer, 1952). Figure 1 illustrates this waviness by means of the surface of the upper part of the trachea, which was segmented from a high-resolution three-dimensional (3D) magnetic resonance imaging (MRI) scan of a female speaker that produced the tense vowel /i:/ (Birkholz *et al.*, 2020). The supplementary material,[1] furthermore, includes a video showing how the waviness changes when the trachea is stretched or compressed. Therefore, tracheas are similar to wavy-walled tubes, which have been studied to some extent in different contexts (Nishimura *et al.*, 2003). However, we are not aware of any morphometric studies that quantified the wave patterns of the human trachea. According to our own preliminary measurements, the depth of the waves is in the range of 1–2 mm.

In this study, we investigated how the ripple depth of wavy-walled tracheas affects important parameters of phonation. To this end, physical trachea models with ripple depths of 0 mm (smooth walls), 1 mm, and 2 mm were used in combination with three different synthetic vocal fold models. The pressures for the phonation onset and offset, along with the mean flow and the fundamental frequency of vocal fold oscillation, were determined and analyzed.

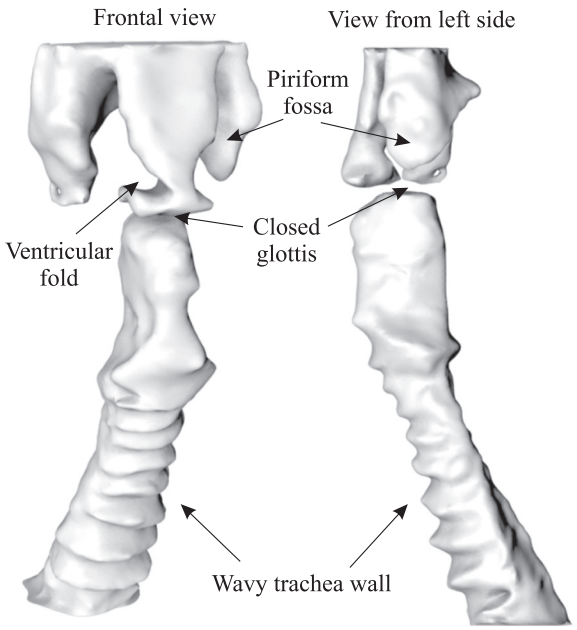

FIG. 1. Near-frontal view and side view of the upper part of a human trachea (the inner walls) extracted from high-resolution 3D magnetic resonance images.

II. METHOD

A. Experimental setup

The complete experimental setup is shown in Fig. 2. The airflow was provided by a fan (U71HL-024 KM-4, Micronel, Tagelswangen, Switzerland) and directed into an air tank (sound-insulated with 25 mm acoustic foam) with an inner volume of $30 \times 30 \times 50\,\mathrm{cm}^3$. Because the fan power could only be controlled in small discrete steps, a self-constructed servo valve was used as a bypass for the fine tuning of the generated air pressure. The air tank with the fan and valve were placed in a soundproofed chamber for noise reduction. A 2.2 m long tube with an inside diameter of 19 mm connected the air tank to another lung-like sound-insulated box with inner dimensions of $25 \times 25 \times 25\,\mathrm{cm}^3$. A flowmeter (AWM720-P1, Honeywell, Charlotte, North Carolina) measured the volume velocity between the two chambers. The lung box, together with the attached "bronchial horn" were intended to further reduce noise from the air supply and approximate an open-ended termination for the connected tracheal tube (Zhang *et al.*, 2009).

A detailed view of the setup downstream from the lung box is given in Fig. 3. It includes modules for the bronchial horn, the trachea, an adaptor section, the vocal folds, and the vocal tract. The module numbers and their corresponding cross-sections are provided on the left and right,

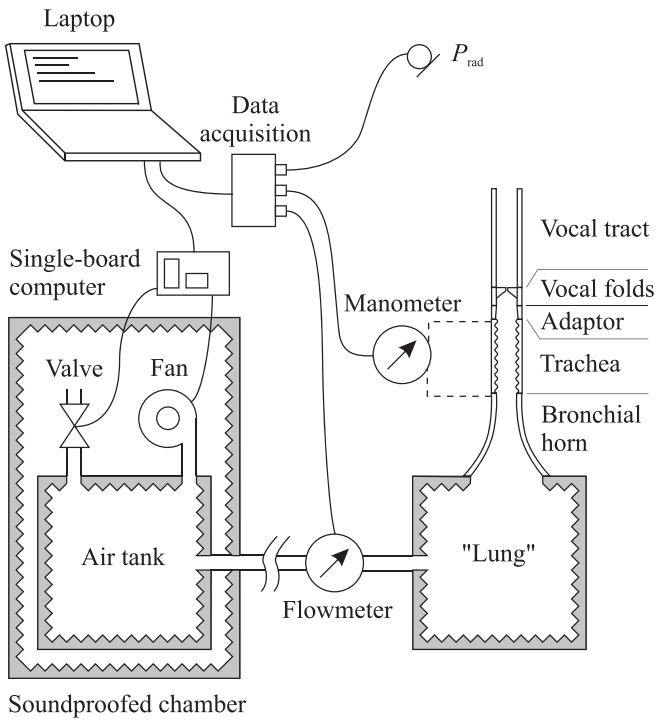

FIG. 2. Complete setup of the measurement system.

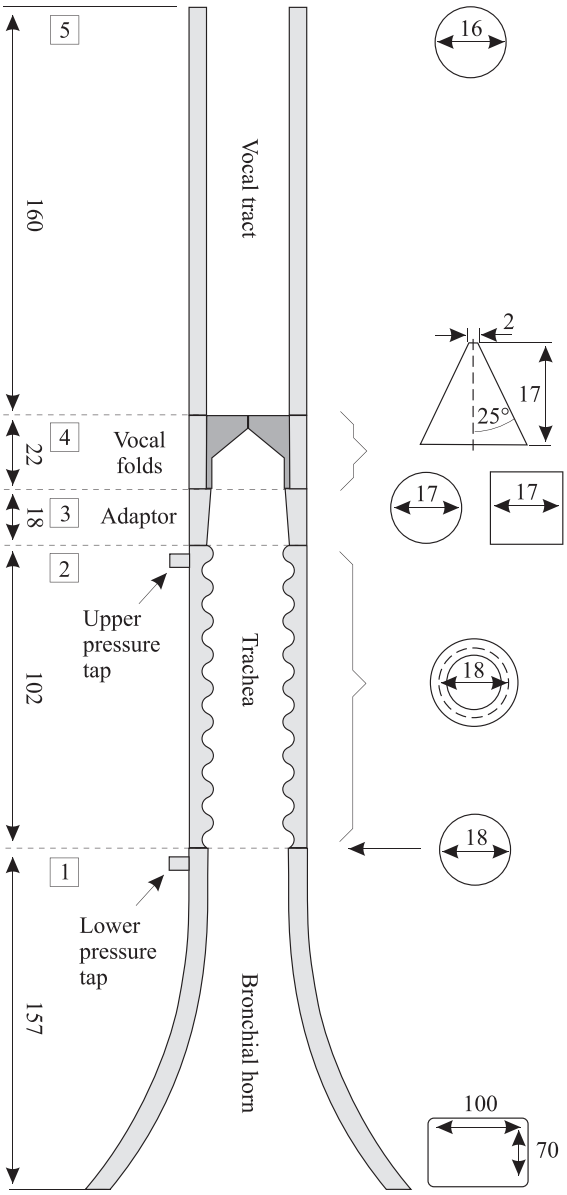

FIG. 3. Detailed scheme of the modular structure of the subglottal system, the vocal folds, and the vocal tract. Module numbers and lengths are shown on the left, and cross-sections are shown on the right. For the larynx module (4), there were three types with triangular, circular, and quadratic shapes. All units are given in mm.

respectively. All modules (except the vocal folds, which consist of multiple materials) have been created using 3D-printing with the material polylactic acid (PLA) using an Ultimaker 3 printer (Ultimaker B.V., Utrecht, Netherlands) with 100% infill (solid walls). The bronchial horn tapered the cross section from a lower rectangular area of $7 \times 10\,\mathrm{cm}^2$ to an upper circular area of $2.54\,\mathrm{cm}^2$. These areas of the bronchial horn correspond to the total cross-sectional areas of the human airway model by Weibel (1963, Table XI.2) of the branch generations 14 and 0, respectively. To measure the pressure at the lower end of the trachea, a pressure tap has been used at the upper end of the bronchial horn. This pressure tap was connected to a differential manometer (DMU4, Kalinsky Sensor Elektronik, Erfurt, Germany).

Stacked on top of the bronchial horn were a trachea model, an adaptor, a vocal fold model, and a vocal tract resonator. For the trachea, three variants with different degrees of wall ripple were used as described in detail in Sec. II B. All trachea modules had a pressure tap 9 mm below the upper end to measure the pressure right below the glottis (see Fig. 2).

The vocal folds were made in three variants with different profiles in the glottic plane as indicated at the right side of Fig. 3. The design and fabrication of the vocal folds is described in detail in Sec. II C. For each vocal fold model, an individual adaptor was used to smoothly change the circular area of the trachea to the cross section of the corresponding vocal fold model.

The vocal tract, which was attached on top of the vocal folds for some of the measurements, was a 160 mm long tube in which the cross section smoothly changed from the specific geometry of the used vocal fold model to a circular cross section with a diameter of 16 mm at the upper end. All modules were screwed together with flanges and sealed with silicon rings. The geometry files of all parts created via 3D-printing in Fig. 3 are contained in the supplementary materials for easy reproduction.[1]

To measure the acoustic output of the setup, a microphone (MV210 with microphone capsule MK250, RFT VEB microphone technology, Dresden, Germany) was placed 30 cm above and 30 cm laterally from the upper end of the vocal tract (to prevent the airstream from impinging on the microphone membrane). The analog signals from the microphone, manometer, and flowmeter were synchronously digitized with a four-channel data acquisition device (DataTranslation 9837C, Norton, MA) at a sampling rate of 48 kHz with 24 bits quantization per channel, transmitted to a laptop computer, and stored to hard disk with custom-made software.

B. Design and fabrication of the trachea modules

As stated in Sec. I, a typical trachea is formed by 12–20*C*-shaped tracheal rings that are vertically connected by ligaments (Breatnach *et al.*, 1984; Kamel *et al.*, 2009; Premakumar *et al.*, 2018). It can be longitudinally stretched and compressed by different degrees to form a more or less wave-like wall pattern. At the top of the trachea is the cricoid cartilage, which connects the trachea to the larynx. The average length of the trachea, including the cricoid, is about 12 cm for male adults (Weibel, 1963). In our setup, the cricoid cartilage was represented by the adaptor module with a length of 18 mm, and the ring sections were represented by the trachea module with a length of $L = 102$ mm (see Fig. 3).

The trachea module was designed as a straight tube with circular cross-sections. To account for the wavy walls, the inner radius r of the tube was modeled as a function of the position x along the tube axis according to

$$r(x) = \bar{r} + \frac{D}{2}\sin(2\pi x/l), \tag{1}$$

https://doi.org/10.1121/10.0003362

where $\bar{r} = 9$ mm is the average radius (Kamel *et al.*, 2009), l is the period length of the wall ripple, and D is the ripple depth. A section of this tube is shown in Fig. 4. The period length l corresponds to the average distance between the tracheal rings and was set to 6 mm for an integer number of 17 rings. These values fall into the typical ranges reported by Kamel *et al.* (2009, Table II). The ripple depth D was varied between 0 mm (smooth walls), 1 mm, and 2 mm, and for each of these values, an individual trachea module was created via 3D-printing. The outer radius R of the tubes was 12 mm in all cases.

C. Design and fabrication of the vocal fold models

To find out whether wavy trachea walls affect phonation similarly for different types of vocal fold models, three vocal fold models were created. The three models differed in terms of their profiles in the glottic plane, which are shown on the right side of Fig. 3. They have a square, a circular, and a triangular profile. Rectangular profiles are the most common in the literature (Chen *et al.*, 2008; Mendelsohn and Zhang, 2011; Murray and Thomson, 2011), and the corresponding vocal folds have a uniform coronal cross section along the whole dorso-ventral length. Round profiles are somewhat more similar to human vocal folds and can be more easily connected to subglottal or supraglottal tubes with circular cross-sections without the need for adaptors or risking unwanted turbulence when cross-sections change abruptly (Birkholz *et al.*, 2019a; Honda *et al.*, 2011). Triangular profiles are probably the most realistic as they reflect the shape of the thyroid cartilage. Here, we used an angle of 25° between the midline and the left and right side walls, which is close to the value of 30° of the MRI-based vocal fold model used by Bouvet *et al.* (2021). The glottis length was 17 mm in all models, which is a typical length for male adults (Zhang, 2016).

The coronal profile was based on the established M5 geometry by Scherer *et al.* (2001) for each model, which is shown in Fig. 5. For the circular and triangular shapes, where the vocal fold width changes in the dorso-ventral direction, Fig. 5 shows the profile at the mid-point of the glottis and at the posterior end, respectively. All vocal folds have a three-layer structure based on Murray and Thomson (2012), consisting of a relatively stiff body layer, a soft,

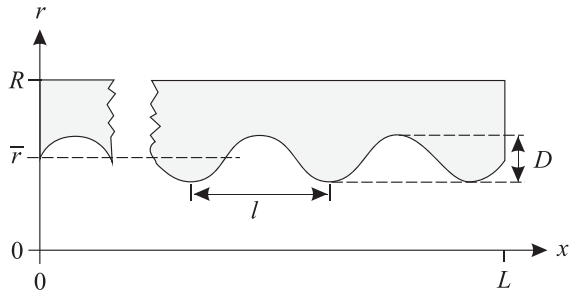

FIG. 4. Details of the trachea module (2) in Fig. 3. The inner radius of the trachea varies as a sine function with a wavelength that represents the distance between two adjacent cartilaginous tracheal rings.

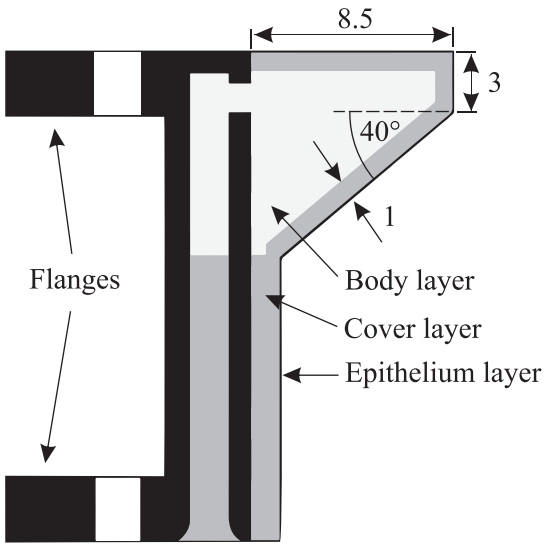

FIG. 5. Coronal cross section of the larynx modules where the width of the vocal folds is widest (here, 8.5 mm). Each vocal fold consists of a body layer, a cover layer, and an epithelium layer.

1 mm thick cover layer, and a very thin and stiff epithelium layer.

All three layers were fabricated by mixing a two-component silicone compound solution (EcoFlex 00-30, SmoothOn, Macungie, PA, supplied by KauPo, Spaichingen, Germany) with different amounts of EcoFlex thinner to obtain different degrees of stiffness. The body layer was created with a weight ratio of 1:1:4 of the components *A* and *B* of the EcoFlex 00–30 (one part each) and the thinner (four parts). According to Murray (2011), the resulting material has a Young's modulus of 2.08 kPa, which is close to the value of 2 kPa measured for the human vocalis muscle (Chhetri *et al.*, 2011). The cover layer was created with a weight ratio of 1:1:6 of the three components. According to Gabriel *et al.* (2019), this material has a Young's modulus of 1.1 kPa, which is similar to that of the human mucosa (Alipour and Vigmostad, 2012). The epithelium layer was created with a weight ratio of 1:1:0, i.e., without using the thinner, for a Young's modulus of 60 kPa (Xuan and Zhang, 2014).

For the fabrication of the vocal folds, the support structures for the different models were designed and created via 3D-printing with the material PLA using an Ultimaker 3 printer [Ultimaker B.V., Utrecht, Netherlands; Figs. 6(a)–6(c)]. Furthermore, to cast the silicone mixtures for the body and cover layers, negatives of these layers were designed and created via 3D-printing with the water-soluble material polyvinyl alcohol (PVA) using an Ultimaker 3 printer [Figs. 6(d) and 6(g)]. The Standard Triangle Language (STL) files of all shapes are available in the supplementary material.[1] After 3D-printing all of these parts, the individual vocal folds were fabricated as follows. The support structure and the negative for the body layer were glued together with a water-soluble adhesive [Fig. 6(e)]. The silicone mixture for the body layer was poured into the resulting mold and cured for 24 h. The body-layer negative

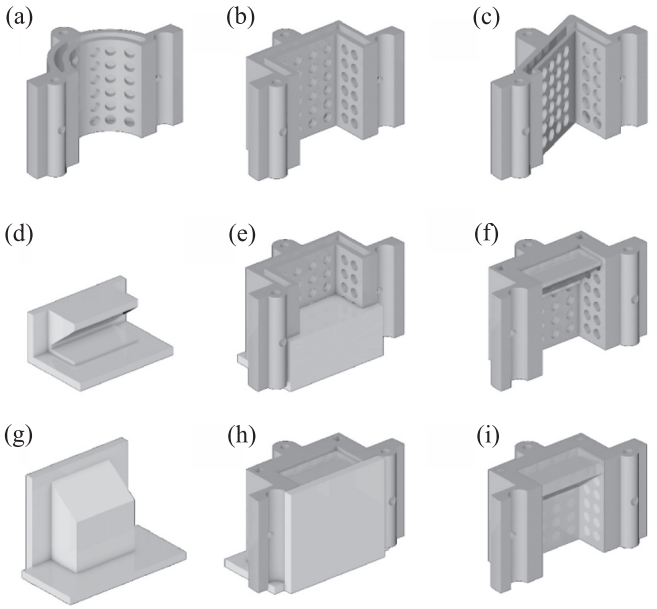

FIG. 6. Illustration of the fabrication of the silicone vocal fold models and their supports. (a)–(c) Support structures for the circular, quadratic, and triangular vocal folds. (d) The water-soluble negative for the fabrication of the body layer of a rectangular vocal fold, (e) the positive and negative glued together, (f) the finished body layer, (g) the water-soluble negative for the fabrication of the cover layer, (h) the positive and negative glued together, and (i) the finished cover layer.

was then dissolved in water, and the cover-layer negative was glued to the support structure [Fig. 6(h)]. The silicone mixture for the cover layer was poured into the resulting mold and cured for 24 h. The cover-layer negative was then dissolved in water [Fig. 6(i)]. Before applying the final epithelium layer, the cover layer was dipped in talcum powder and tapped until no more lumps adhered. According to Gabriel *et al.* (2019), the talcum powder between the two layers reduces the surface stickiness and waviness of the epithelium. A few drops of the silicone mixture for the epithelium layer were dropped over the powdered cover layer. Then, the whole model was positioned at an angle to let the silicone run off (except the very thin layer) and cured for another 24 h.

D. Measurements

For each combination of the three trachea modules (with surface ripple depths of $D = 0$ mm, $D = 1$ mm, and $D = 2$ mm) with the three vocal fold models (square, circular, and triangular), the phonation onset pressure, the phonation offset pressure, the fundamental frequency (f_0), and the mean flow were measured as follows. Starting at the lowest value, the power of the fan was incremented in small steps (corresponding to subglottal pressure steps of about 8 Pa) until a stable vocal fold oscillation was reached. After each pressure step, a pause of about 3 s was made before the next step to allow the vocal fold vibration to establish itself. When a stable oscillation was established, the *onset* pressures at the lower and upper ends of the trachea were determined relative to atmospheric pressure. Then, the fan power was reduced in small steps until the vibration stopped again. In this state, the *offset* pressures at the lower and upper ends of the trachea were determined. To determine f_0, the pressure was increased again to a value of about 100 Pa above the onset pressure. In this state, 10 s of the audio signal were recorded from which the average f_0 was determined with the software Praat (Boersma and Weenik, 2017). The mean flow was determined both at the onset and offset pressures. For each measurement, the pressure and flow values were averaged over a time of 10 s.

For each combination of trachea and vocal fold models, the measurements were performed three times with a vocal tract and three times without a vocal tract. The order of the measurements was randomized in such a way that the combination of trachea and vocal fold model changed after each measurement.

To rule out a possible influence of the turbulence at the wavy trachea walls on the pressure measurements, validation measurements were performed with a thin cannula (inner diameter of 0.1 mm) inserted up to the center of the trachea at the position of the upper pressure tap as shown in Fig. 7. The end of the cannula was connected to the same device that was used to make the "regular" pressure measurements. For the purpose of validation, it was sufficient to repeat measurements for only two situations (circular vocal folds without a vocal tract and triangular vocal folds with a vocal tract).

Finally, to determine the effect of the trachea wall ripple on the acoustic properties of the subglottal system, the input impedance of the subglottal system has been measured for the three trachea modules. The measurement setup is shown in Fig. 8 and used an impedance sensor with a baffled loudspeaker (Dalmont, 2001; Singh and Schary, 1978). The housing parts of the sensor were created via 3D-printing with PLA analogous to the trachea modules. The loudspeaker (VECO 32KC08-1A, New Taipei City, Taiwan) was placed at the position of the glottis to excite the subglottal system with a sine sweep. During the excitation, the sound pressure was measured with a 1/4 in. measurement microphone (G.R.A.S. 46BL, GRAS Sound & Vibration, Holte, Denmark) immediately below the loudspeaker (P_1) and in an airtight enclosure around the back of the loudspeaker (P_2). For low frequencies, the pressure in the enclosure is uniform and related to the volume velocity U generated by the loudspeaker with $U(\omega) \propto j\omega P_2(\omega)$ (Singh and Schary, 1978) so that the input impedance of the subglottal system could be calculated as $P_1/(j\omega P_2)$, where $j = \sqrt{-1}$ and ω is the angular frequency. For synchronous playback and recording, a Universal Serial Bus (USB) audio

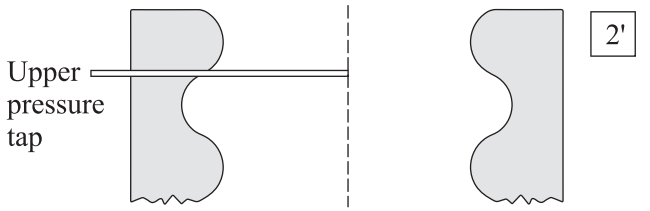

FIG. 7. Modification of the trachea module with a cannula inserted at the upper pressure tap.

https://doi.org/10.1121/10.0003362

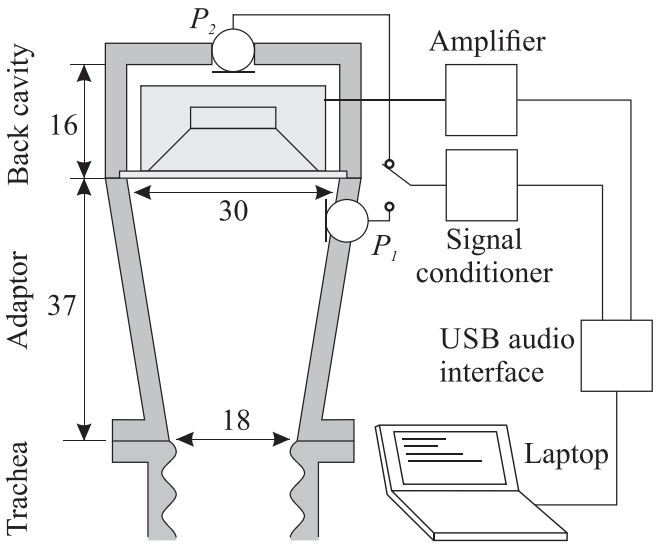

FIG. 8. Setup to determine the input impedance of the subglottal system from the position of the glottis.

interface (Terratec XFire 8HD, Alsdorf, Germany) was used. The excitation signal was fed to the loudspeaker via an amplifier (Kemo M032S, Dartford, Kent, UK), and the microphones were powered with a signal conditioner (M208A, Metra Mess- und Frequenztechnik, Radebeul e.K.). The measurements were performed with the open-source software MeasureTransferFunction (Birkholz, 2019), which is based on the method by Farina (2000) and uses a sampling rate of 96 000 Hz and a quantization of 24 bit. The excitation signal was a logarithmic sine sweep with a power band from 50 to 10 000 Hz (fade-in and fade-out from 20 to 50 Hz and 10 000–11 000 Hz, respectively) and a duration of 10.4 s.

III. RESULTS

A. Pressure and flow values at phonation onset and offset

The measurements of the phonation onset and offset pressures for all conditions are shown in Fig. 9 for the setup *with* a vocal tract and in Fig. 10 for the setup *without* a vocal tract. The left and right panels in Figs. 9 and 10 show the measurements at the lower and upper ends of the trachea, respectively. Each data point in Figs. 9 and 10 is the mean value of the three measurement runs per condition, and the square, round, and triangular symbols indicate the respective vocal fold shapes. Onset pressure values are connected with solid lines, and offset pressure values are connected with dashed lines.

The pressures at the lower end of the trachea appear to be rather independent from the wall ripple depth D, although there is a slight tendency for lower pressures at higher ripple depths. However, the pressures directly below the glottis clearly drop with increasing wall ripple. *With* a vocal tract, the onset (offset) pressures at the upper end of the trachea with $D = 2$ mm drop, compared to $D = 0$ mm (smooth walls), by 17.3% (19.3%), 19.2% (20.1%), and 18.5% (19.6%) for the circular, square, and triangular vocal fold models, respectively. *Without* a vocal tract, the onset (offset) pressures at the upper end of the trachea with $D = 2$ mm drop, compared to $D = 0$ mm (smooth walls), by 17.0% (16.9%), 19.5% (18.4%), and 7.9% (8.8%) for the circular, square, and triangular vocal fold models, respectively. The triangular vocal folds used without a vocal tract showed a somewhat abnormal oscillation with a high-frequency secondary oscillation of the lower vocal fold edge, which may explain the difference in the pressure drop compared to the other models and conditions.

Although the *relative* pressure drops, occurring with increasing wall ripple depth, were independent from the presence or absence of a vocal tract, the *absolute* onset and offset pressures were about 400–500 Pa lower when a vocal tract was used. This effect of a reduced oscillation threshold pressure due to the inertance of the air column in the vocal tract is well known (Titze, 1988). The *absolute* pressure values also depend on the type of vocal fold model. Here, the highest pressures are needed for the square model, and the least pressures are needed for the triangular model with the round model in between.

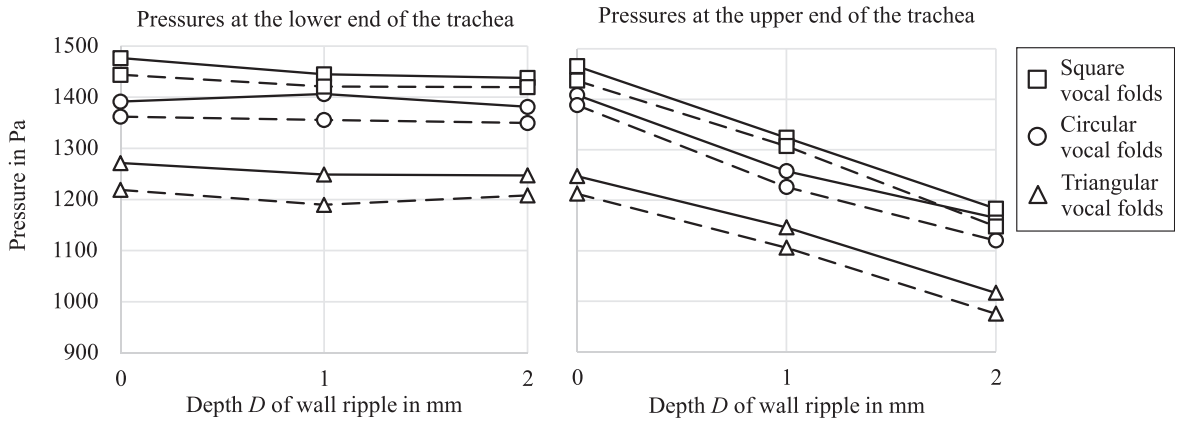

FIG. 9. Phonation onset pressures (solid lines) and offset pressures (dashed lines) for different vocal fold shapes (triangular, circular, and squared as indicated by the symbols) and depths of the trachea wall ripple at the lower and upper pressure taps (left and right, respectively) *with* a vocal tract. Each data point is the average value of three measurement runs.

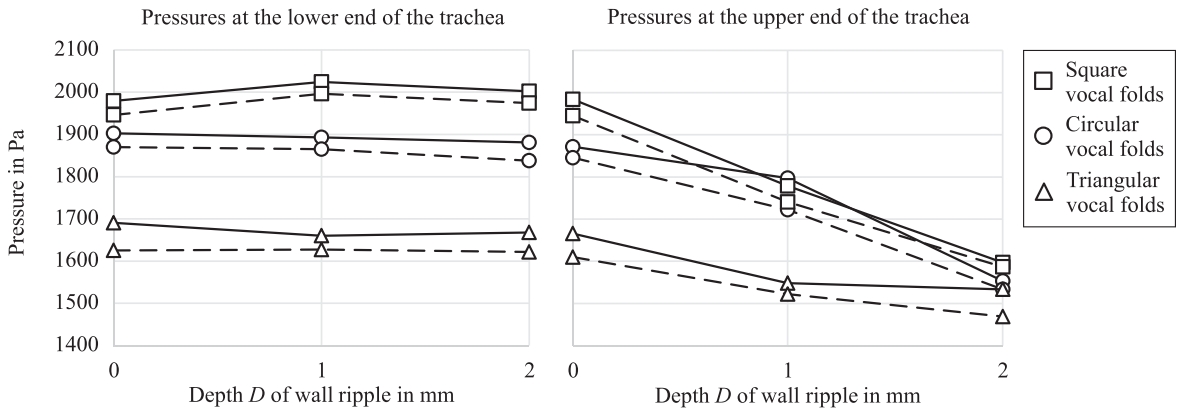

FIG. 10. Phonation onset pressures (solid lines) and offset pressures (dashed lines) for different vocal fold shapes (triangular, circular, and squared as indicated by the symbols) and depths of the trachea wall ripple at the lower and upper pressure taps (left and right, respectively) *without* a vocal tract. Each data point is the average value of three measurement runs.

Figure 11 shows the results of the validation measurements of the onset and offset pressures as a function of the wall ripple depth for the circular vocal folds without a vocal tract and the triangular vocal folds with a vocal tract. Here, the pressures dropped by 14.5% (triangular vocal folds) and 14.2% (circular vocal folds) for $D = 2$ mm compared to $D = 0$ mm. These values, which were obtained at the middle of the tracheal tube, are a little smaller than those obtained at the trachea walls (18.5% and 17.0%) but generally confirm the findings above.

In summary, with increasing depth of the wall ripple, the subglottal onset pressure (at the upper pressure tap) consistently dropped, independently from the presence or absence of a vocal tract and from the used vocal fold model. For the lower pressure tap, there was merely an indication for a pressure drop with increasing wall ripple but not a clear trend. However, a similar trend was seen for the *flow* values across the different conditions, i.e., increasing wall ripple tended to reduce the average flow needed for the phonation onset. With a vocal tract, and averaged across onset and offset conditions and vocal fold models, the flow reduced by $4.4 \pm 2.7\%$ for $D = 2$ mm compared to $D = 0$ mm. Without a vocal tract, flow values were partly not available because the flow exceeded the maximum value of 3333 cm^3/s of the flowmeter. In absolute terms, the flow rates at the phonation onset strongly depended on the type of glottis model and ranged between 1036 and 1196 cm^3/s for the square vocal folds, between 696 and 764 cm^3/s for the circular vocal folds, and between 188 and 224 cm^3/s for the triangular vocal folds (with a vocal tract attached). For comparison, the average flow rates during human phonation range from 120 to over 500 cm^3/s, depending on the phonation type (Ladefoged, 1988).

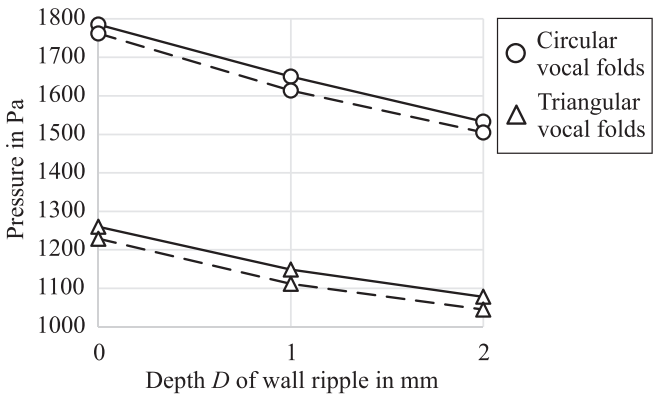

FIG. 11. Validation measurements for the oscillation onset pressures (solid lines) and offset pressures (dashed lines) measured at the upper end of the trachea using the cannula as shown in Fig. 7. The circles represent values measured for the circular larynx (without a vocal tract), and the triangles represent values measured for the triangular larynx (with a vocal tract).

B. Fluid power

Since both the pressure (at the lower pressure tap) and the flow showed the tendency to decrease with increasing trachea wall ripple, this tendency should be even more evident in the fluid power values, which are the product of pressure and flow. In Fig. 12, these values have been plotted for the phonation onset (individually for all three measurement runs per condition) for the three vocal fold models and the

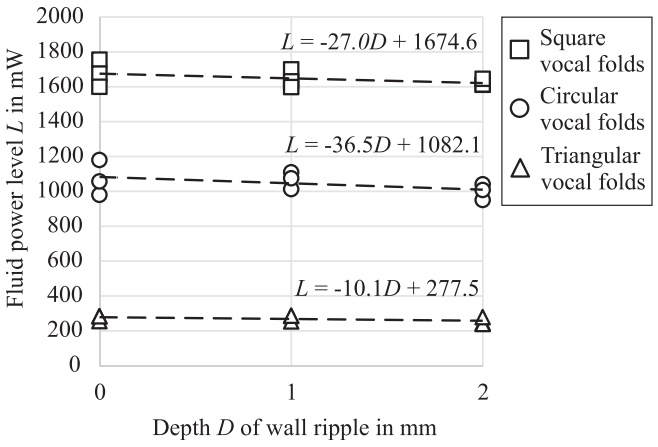

FIG. 12. Pulmonary power (pressure × flow) at phonation onset measured at the lower end of the trachea for the different depths of trachea wall ripple and vocal fold shapes (triangular, circular, and squared as indicated by the symbols) from all three measurement runs. For each larynx shape, a regression line was fitted through the nine corresponding points.

https://doi.org/10.1121/10.0003362

three wall ripple depths and fitted with regression lines. The slopes of the regression lines are negative for all three vocal fold models and indicate that the pulmonary power needed to initiate phonation also reduced with the depth of the trachea wall ripple. However, none of the slopes was significantly different from zero according to a linear regression *t*-test ($p > 0.05$ for all three lines). Yet, strong differences of the fluid power between the vocal fold models can be noted, which range from about 250 mW for the triangular shape to over 1600 mW for the square shape.

C. Fundamental frequency

The fundamental frequencies of the vocal fold oscillations for the different conditions are shown in Fig. 13. There was no dependency of f_0 on the depth of the wall ripple. However, the vocal fold shapes and the presence or absence of a vocal tract had an effect. The triangular vocal folds had the highest f_0, the square vocal folds had the lowest f_0, and the f_0 of the circular vocal folds was in between. The f_0 values with a vocal tract (solid lines) were higher than the values without a vocal tract (dashed lines) for all three models. The f_0 values obtained with the triangular vocal folds with a vocal tract strongly differed from the other measurements due to the abnormal oscillation mode as mentioned in Sec. III A.

D. Input impedance of the subglottal system

The magnitude spectra of the input impedance of the subglottal system are shown in Fig. 14 for the three depths D of the trachea wall ripple. The strong similarity of the spectra indicates that the ripple depth hardly affected the acoustic properties of the subglottal system, especially at low frequencies. The first resonance frequency was close to 310 Hz in all three cases and, hence, considerably higher than the f_0 of the vocal fold oscillations. However, it is

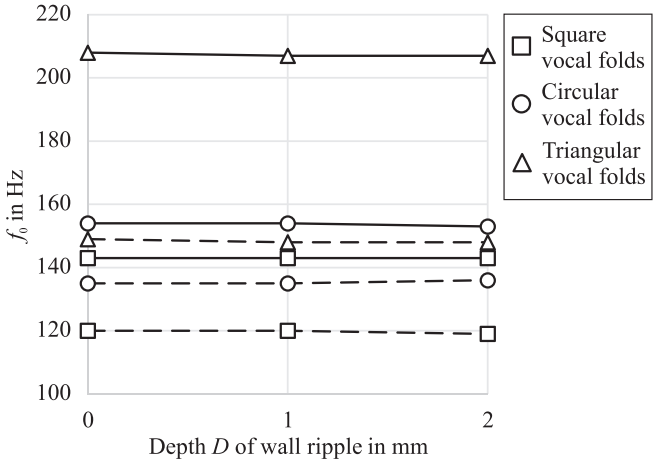

FIG. 13. Fundamental frequency of vocal fold oscillation as a function of the depth of the trachea wall ripple and the vocal fold shape (triangular, circular, and square, according to the symbols). Each symbol represents the average value of three measurement runs. The symbols connected with solid and dashed lines represent f_0 values with and without a vocal tract, respectively.

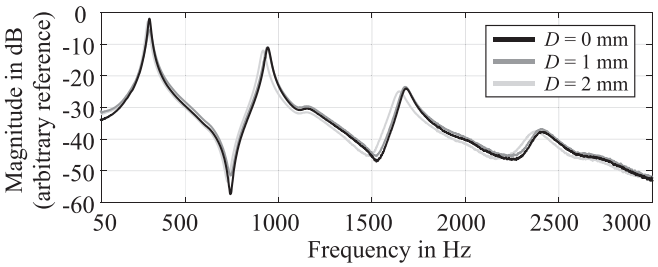

FIG. 14. Input impedance of the subglottal system as seen from the position of the vocal folds for the different depths D of the trachea wall ripple.

lower than that of the *human* subglottal system (around 600 Hz, according to Ishizaka *et al.*, 1976), although the dimensions of the trachea modules and the bronchial horn were based on anatomical data by Weibel (1963). This discrepancy is likely caused by the hard trachea walls of our physical setup (compared to the soft walls of the real subglottal system) as it has been shown with computer simulations by Ishizaka *et al.* (1976) and Ho *et al.* (2011).

IV. DISCUSSION AND CONCLUSIONS

This study demonstrated that the phonation onset and offset pressures closely below the glottis (subglottal pressures) are affected by the waviness of the trachea walls. Compared to smooth walls, a ripple depth of 2 mm caused the pressures to drop by up to 20%. This effect was shown to be independent from the geometry of the vocal folds and from the presence or absence of a vocal tract.

The pressures at the *lower* end of the trachea, i.e., the lung pressure, remained approximately constant for smooth and rippled trachea walls. Therefore, the pressure drop across the trachea and, accordingly, the flow resistance increased with increasing wall ripple. This suggests that the flow in the trachea becomes increasingly turbulent with increasing wall ripple.

Trachea wall ripple also slightly reduced the average flow needed to initiate vocal fold oscillation. The pulmonary power (the product of flow and lung pressure) needed to initiate phonation, thus, tended to decrease with increasing wall ripple; however, the obtained results were not significant. The fundamental frequency was not affected by the ripple of the trachea walls.

The type of vocal fold model and the presence or absence of a vocal tract did not affect the *relative* drop of the pressure and flow measures with increasing trachea wall ripple. However, in absolute terms, phonation onset and offset pressures were higher when no vocal tract was attached to the vocal folds, which is in line with theoretical findings (Titze, 1988). Furthermore, the highest pressures were required for the square vocal fold models, followed by the circular and triangular models. These differences were also reflected by the pulmonary powers needed to initiate phonation with about 1650 mW, 1150 mW, and 250 mW for the square, round, and triangular vocal fold models, respectively. A pulmonary power of 250 mW is much more representative for human phonation than are the higher values

(Titze, 2018), hence, the triangular vocal fold model can be regarded as the most realistic model in this respect.

The reason for the reduction of the phonation onset pressure with increasing trachea wall ripple is not entirely clear yet. Because the input impedance of the subglottal system was rather independent from the trachea wall ripple and the first subglottal resonance was considerably higher than the f_0 of the vocal fold models, subglottal acoustics as discussed by Zhang *et al*. (2006) seem not to be a likely cause. We suggest that an increasing degree of turbulence or unsteady flow effects with increasing wall ripple trigger oscillation onset at lower pressures. According to Dekker (1961), the transition from laminar to turbulent flow in the trachea starts at a flow rate of about 122 cm^3/s. This value was not only exceeded in our experiments but is also exceeded during human phonation (at least during part of the glottal cycles) with average flow rates between 120 cm^3/s and over 500 cm^3/s, depending on the phonation type (Ladefoged, 1988; Stevens, 1998).

In conclusion, the observations in this study suggest that geometric details of the subglottal system and the flow conditions in the trachea may have a more important effect on phonation than previously thought. It can be speculated that the flexibility of the human trachea in terms of bending, streching, and compression (along with the changes of the wall ripple) even provides a mechanism to facilitate or impede vocal fold oscillation. This would complement other factors that affect the ease of phonation such as the velocity of the mucosal wave, the pre-phonatory gap between the vocal folds (Titze, 1988), or the viscosity of the vocal fold mucosa (Finkelhor *et al*., 1988; Titze *et al*., 1995).

However, both the trachea and vocal fold models used in this study are based on multiple simplifications compared to their real counterparts. The vocal fold models, for example, did not represent the anisotropic properties of real vocal folds, and the wavy walls of the trachea model did not consider the more or less smooth posterior part formed by the membranous wall that contains the trachealis muscle. Future studies are needed to explore the impact of more realistic models on the relevant parameters of phonation and to better understand the mechanisms underlying the presented observations.

[1]See supplementary material at https://www.scitation.org/doi/suppl/10.1121/10.0003362 for a video showing the wall ripple of the trachea and CAD files for the measurement setup. The supplementary material can also be found at https://www.vocaltractlab.de/index.php?page=birkholz-supplements (Last viewed 1/13/21).

Alipour, F., and Vigmostad, S. (**2012**). "Measurement of vocal folds elastic properties for continuum modeling," J. Voice **26**(6), 816.e21–816.e29.

Birkholz, P. (**2019**). "MeasureTransferFunction [software]," available at https://www.vocaltractlab.de/index.php?page=measuretransferfunction-download (Last viewed 1/13/21).

Birkholz, P., Gabriel, F., Kürbis, S., and Echternach, M. (**2019a**). "How the peak glottal area affects linear predictive coding-based formant estimates of vowels," J. Acoust. Soc. Am. **146**(1), 223–232.

Birkholz, P., Kürbis, S., Stone, S., Häsner, P., Blandin, R., and Fleischer, M. (**2020**). "Printable 3D vocal tract shapes from MRI data and their acoustic and aerodynamic properties," Sci. Data **7**(1), 1–16.

Birkholz, P., Stone, S., and Kürbis, S. (**2019b**). "Comparison of different methods for the voiced excitation of physical vocal tract models," in *Study Texts in Speech Communication: Electronic Speech Signal Processing*, edited by P. Birkholz and S. Stone (TUDpress, Dresden), pp. 84–94.

Boersma, P., and Weenik, D. (**2017**). "Praat: Doing phonetics by computer (version 6.1.09) [computer program]," http://www.praat.org/ (Last viewed 1/13/21).

Bouvet, A., Tokuda, I., Pelorson, X., and Van Hirtum, A. (**2021**). "Imaging of auto-oscillating vocal folds replicas with left–right level difference due to angular asymmetry," Biomed. Signal Process. Control **63**, 102154.

Breatnach, E., Abbott, G. C., and Fraser, R. G. (**1984**). "Dimensions of the normal human trachea," Am. J. Roentgenol. **142**(5), 903–906.

Burks, G., Singh, M., De Vita, R., Johnson, B., and Leonessa, A. (**2020**). "Effect of mechanical properties on the dynamics of self-oscillating synthetic vocal folds," J. Dyn. Syst., Meas., Control **143**(2), 021001.

Chen, L.-J., Zañartu, M., Cook, D., and Mongeau, L. (**2008**). "Effects of acoustic loading on the self-oscillations of a synthetic model of the vocal folds," in *Proc. of the Ninth International Conference on Flow-Induced Vibrations*, Vol. 30, pp. 1–6.

Chhetri, D. K., Zhang, Z., and Neubauer, J. (**2011**). "Measurement of Young's modulus of vocal folds by indentation," J. Voice **25**(1), 1–7.

Choi, J., Tawhai, M. H., Hoffman, E. A., and Lin, C.-L. (**2009**). "On intra- and intersubject variabilities of airflow in the human lungs," Phys. Fluids **21**(10), 101901.

Dalmont, J.-P. (**2001**). "Acoustic impedance measurement, Part I: A review," J. Sound Vib. **243**(3), 427–439.

Dekker, E. (**1961**). "Transition between laminar and turbulent flow in human trachea," J. Appl. Physiol. **16**(6), 1060–1064.

Farina, A. (**2000**). "Simultaneous measurement of impulse response and distortion with a swept-sine technique," in *Audio Engineering Society Convention 108*.

Finkelhor, B. K., Titze, I. R., and Durham, P. L. (**1988**). "The effect of viscosity changes in the vocal folds on the range of oscillation," J. Voice **1**(4), 320–325.

Fischer, H. (**1952**). "Beitrag zur funktionellen Struktur der Trachea" ("Contribution to the functional structure of the trachea"), Anatomischer Anzeiger (Anat. J.) **99**, 277–286.

Fukui, K., Ishikawa, Y., Shintaku, E., Honda, M., and Takanishi, A. (**2012**). "Production of various vocal cord vibrations using a mechanical model for an anthropomorphic talking robot," Adv. Rob. **26**(1-2), 105–120.

Gabriel, F., Häsner, P., Dohmen, E., Borin, D., and Birkholz, P. (**2019**). "Stickiness and surface waviness of two-layer silicone rubber structures for synthetic vocal folds," in *Study Texts in Speech Communication: Electronic Speech Signal Processing*, edited by P. Birkholz and S. Stone (TUDpress, Dresden), pp. 221–230.

Ho, J. C., Zañartu, M., and Wodicka, G. R. (**2011**). "An anatomically based, time-domain acoustic model of the subglottal system for speech production," J. Acoust. Soc. Am. **129**(3), 1531–1547.

Honda, M., Fukui, K., Ogane, R., and Takanishi, A. (**2011**). "Pathological voice production by mechanical vocal cord model," in *Proc. of the 9th International Seminar on Speech Production*, pp. 49–56.

Ishizaka, K., Matsudaira, M., and Kaneko, T. (**1976**). "Input acoustic-impedance measurement of the subglottal system," J. Acoust. Soc. Am. **60**(1), 190–197.

Kamel, K. S., Lau, G., and Stringer, M. D. (**2009**). "*In vivo* and *in vitro* morphometry of the human trachea," Clin. Anat. **22**(5), 571–579.

Kniesburges, S., Birk, V., Lodermeyer, A., Schützenberger, A., Bohr, C., and Becker, S. (**2017**). "Effect of the ventricular folds in a synthetic larynx model," J. Biomech. **55**, 128–133.

Ladefoged, P. (**1988**). "Discussion of phonetics: A note on some terms for phonation types," in *Vocal Physiology: Voice Production*, edited by O. Fujimura (Raven, New York), pp. 373–375.

McPhail, M. J., Campo, E. T., and Krane, M. H. (**2019**). "Aeroacoustic source characterization in a physical model of phonation," J. Acoust. Soc. Am. **146**(2), 1230–1238.

Mendelsohn, A. H., and Zhang, Z. (**2011**). "Phonation threshold pressure and onset frequency in a two-layer physical model of the vocal folds," J. Acoust. Soc. Am. **130**(5), 2961–2968.

Migimatsu, K., and Tokuda, I. T. (**2019**). "Experimental study on nonlinear source–filter interaction using synthetic vocal fold models," J. Acoust. Soc. Am. **146**(2), 983–997.

Murray, P. R. (**2011**). "Flow-induced responses of normal, bowed, and augmented synthetic vocal fold models," Masters thesis (Brigham Young University, Provo, UT).
Murray, P. R., and Thomson, S. L. (**2011**). "Synthetic, multi-layer, self-oscillating vocal fold model fabrication," J. Visualized Exp. **58**, e3498.
Murray, P. R., and Thomson, S. L. (**2012**). "Vibratory responses of synthetic, self-oscillating vocal fold models," J. Acoust. Soc. Am. **132**(5), 3428–3438.
Nishimura, T., Bian, Y., Matsumoto, Y., and Kunitsugu, K. (**2003**). "Fluid flow and mass transfer characteristics in a sinusoidal wavy-walled tube at moderate Reynolds numbers for steady flow," Heat Mass Transfer **39**(3), 239–248.
Nowak, N., Kakade, P. P., and Annapragada, A. V. (**2003**). "Computational fluid dynamics simulation of airflow and aerosol deposition in human lungs," Ann. Biomed. Eng. **31**(4), 374–390.
Pickup, B. A., and Thomson, S. L. (**2009**). "Influence of asymmetric stiffness on the structural and aerodynamic response of synthetic vocal fold models," J. Biomech. **42**(14), 2219–2225.
Pickup, B. A., and Thomson, S. L. (**2010**). "Flow-induced vibratory response of idealized versus magnetic resonance imaging-based synthetic vocal fold models," J. Acoust. Soc. Am. **128**(3), EL124–EL129.
Premakumar, Y., Griffin, M., and Szarko, M. (**2018**). "Morphometric characterisation of human tracheas: Focus on cartilaginous ring variation," BMC Res. Notes. **11**(1), 32.
Scherer, R. C., Shinwari, D., De Witt, K. J., Zhang, C., Kucinschi, B. R., and Afjeh, A. A. (**2001**). "Intraglottal pressure profiles for a symmetric and oblique glottis with a divergence angle of 10 degrees," J. Acoust. Soc. Am. **109**(4), 1616–1630.
Shaw, S. M., Thomson, S. L., Dromey, C., and Smith, S. (**2012**). "Frequency response of synthetic vocal fold models with linear and nonlinear material properties," J. Speech, Lang., Hear. Res. **55**(5), 1395–1406.
Singh, R., and Schary, M. (**1978**). "Acoustic impedance measurement using sine sweep excitation and known volume velocity technique," J. Acoust. Soc. Am. **64**(4), 995–1003.
Stevens, K. N. (**1998**). *Acoustic Phonetics* (The MIT Press, Cambridge, MA).
Thomson, S. L., Mongeau, L., and Frankel, S. H. (**2005**). "Aerodynamic transfer of energy to the vocal folds," J. Acoust. Soc. Am. **118**(3), 1689–1700.
Titze, I. R. (**1988**). "The physics of small-amplitude oscillation of the vocal folds," J. Acoust. Soc. Am. **83**(4), 1536–1552.
Titze, I. R. (**2018**). "Where has all the power gone? Energy production and loss in vocalization," Speech Commun. **101**, 26–33.
Titze, I. R., Schmidt, S. S., and Titze, M. R. (**1995**). "Phonation threshold pressure in a physical model of the vocal fold mucosa," J. Acoust. Soc. Am. **97**(5), 3080–3084.
Weibel, E. R. (**1963**). *Morphometry of the Human Lung* (Springer, Berlin).
Xuan, Y., and Zhang, Z. (**2014**). "Influence of embedded fibers and an epithelium layer on the glottal closure pattern in a physical vocal fold model," J. Speech, Lang., Hear. Res. **57**(2), 416–425.
Zhang, Z. (**2016**). "Mechanics of human voice production and control," J. Acoust. Soc. Am. **140**(4), 2614–2635.
Zhang, Z., Neubauer, J., and Berry, D. A. (**2006**). "The influence of subglottal acoustics on laboratory models of phonation," J. Acoust. Soc. Am. **120**(3), 1558–1569.
Zhang, Z., Neubauer, J., and Berry, D. A. (**2009**). "Influence of vocal fold stiffness and acoustic loading on flow-induced vibration of a single-layer vocal fold model," J. Sound Vib. **322**(1-2), 299–313.